Journal of Magnetism and Magnetic Materials 390 (2015) 15–19

Contents lists available at ScienceDirect

Journal of Magnetism and Magnetic Materials

journal homepage: www.elsevier.com/locate/jmmm

The coercivity mechanism of Pr–Fe–B nanoflakes prepared by surfactant-assisted ball milling

Wen-Liang Zuo*, Ming Zhang, E. Niu, Xiao-Ping Shao, Feng-Xia Hu, Ji-Rong Sun, Bao-Gen Shen*

State Key Laboratory of Magnetism, Institute of Physics, Chinese Academy of Sciences, Beijing 100190, People's Republic of China

ARTICLE INFO

Article history:
Received 8 January 2015
Received in revised form
31 March 2015
Accepted 21 April 2015
Available online 21 April 2015

Keywords:
Coercivity mechanism
Textured Pr–Fe–B nanoflakes
Surfactant-assisted ball milling
Henkel plots

ABSTRACT

The strong (00*l*) textured $Pr_{12+x}Fe_{82-x}B_6$ (x=0, 1, 2, 3, 4) nanoflakes with high coercivity were prepared by surfactant-assisted ball milling (SABM). The thickness and length of the flakes are mainly in the range of 50 – 200 nm and 0.5 – 2 μm, respectively. A coercivity of 4.16 kOe for $Pr_{15}Fe_{79}B_6$ nanoflakes was obtained, which is the maximum coercivity of $R_2Fe_{14}B$ (R=Pr, Nd) nanoflakes or nanoparticles reported up to now. The results of XRD and SEM for the aligned $Pr_{15}Fe_{79}B_6$ nanoflakes indicate that a strong (00l) texture is obtained and the easy magnetization direction is parallel to the surface of the flakes. The angular dependence of coercivity for aligned sample indicates that the coercivity mechanism of the as-milled nanoflakes is mainly dominated by domain wall pinning. Meanwhile, the field dependence of coercivity, isothermal (IRM) and dc demagnetizing (DCD) remanence curves also indicate that the coercivity is mainly determined by domain wall pinning, and nucleation also has an important effect. In addition, the mainly interaction of flakes is dipolar coupling. The research of coercivity mechanism for $Pr_{15}Fe_{79}B_6$ nanoflakes is important for guidance the further increase its value, and is useful for the future development of the high performance nanocomposite magnets and soft/hard exchange spring magnets.

1. Introduction

Nanostrutured rare-earth permanent magnet (REPM) has attracted much attentions owing to the high performance in nanocomposite magnets and soft/hard exchange coupled magnets [1–3]. Furthermore, the surfactant-assisted ball milling (SABM) method has been found efficiently in synthesis of single phase and textured nanostructured REPM compounds [4], however, the coercivity of that, especially for R–Fe–B (R=Nd, Pr) system, is very low [3,5,6]. In our previous work, the stoichiometric composition of $Pr_{12}Fe_{82}B_6$ nanoflakes with a coercivity of 3.9 kOe was obtained, which is the maximum coercivity of $R_2Fe_{14}B$ (R=Pr, Nd) nanoflakes or nanoparticles reported up to now [7]. However, it is still too low for practical application. It is well known that the coercivity would be enhanced by enriching rare-earth phase into the grain boundary for the R–Fe–B compounds [3,5,8]. Therefore, in this work, the $Pr_{12+x}Fe_{82-x}B_6$ (x=0, 1, 2, 3, 4) nanoflakes were prepared by SABM. In addition, the study of coercivity mechanism of the as-milled nanoflakes is also very important for further guidance increase its value and to develop high performance nanocomposite magnets. Therefore, the coercivity mechanism of the as-milled nanoflakes is also studied by the angular dependence of coercivity for aligned $Pr_{15}Fe_{79}B_6$ nanoflakes/resin composites. In order to further clarify the coercivity mechanism and the possible interaction of the $Pr_{15}Fe_{79}B_6$ nanoflakes, the minor hysteresis loops and recoil loops of unaligned sample are also researched.

2. Experiment

$Pr_{12+x}Fe_{82-x}B_6$ (x=0, 1, 2, 3, 4) compounds were prepared by arc melting in argon using pure metals. The ingots were melted five times to ensure homogeneity and then annealed at 1173 K for a week under vacuum. The annealed ingots were ground down to less than 150 μm as the starting powders. The ball milling experiment was performed for 5 h using a GN-2 ball milling equipment (voltage was 60 V and the rotational speed was about 300 rpm). The weight ratio of balls to powders was 20:1. Oleylamine (80 – 90%) and oleic acid (99%) were used as surfactants. The total amount of surfactants was 20% to the weight of the starting powders (Oleylamine and oleic acid was 1:1). Heptane (99.8%) was used as the carrier liquid. The aligned Pr–Fe–B nanoflakes/resin

---

* Corresponding authors.
E-mail addresses: wlzuo@iphy.ac.cn (W.-L. Zuo), shenbg@aphy.iphy.ac.cn (B.-G. Shen).

http://dx.doi.org/10.1016/j.jmmm.2015.04.073
0304-8853/© 2015 Published by Elsevier B.V.

composite was prepared by mixing the as-milled flake with epoxy resin, and placing them into a 20 kOe magnetic field until the epoxy resin solidifies. The phase structure was examined by the X-ray powder diffraction (XRD) with Cu Kα radiation at room temperature. Morphology was analyzed by scanning electron microscope (SEM). Magnetic properties were measured by a vibrating sample magnetometer with the maximum field of 20 kOe at room temperature.

3. Result and discussion

Fig. 1(a) shows the measured XRD patterns of starting $Pr_{12+x}Fe_{82-x}B_6$ (x=0, 1, 2, 3, 4) compounds powder. It can be seen that it is single phase tetragonal structure for $Pr_{12}Fe_{82}B_6$ compound (x=0), With the increase of Pr element, the diffraction peaks of rare-earth phase appear and the intensity become more and more strong, which agrees with our expectation. The coercivity of as-milled $Pr_{12+x}Fe_{82-x}B_6$ (x=0, 1, 2, 3, 4) nanoflakes are shown in Fig. 1(b). It can be observed that the coercivity first slowly increases then decreases with increasing Pr amount, and reaches a maximum value of 4.16 kOe for $Pr_{15}Fe_{79}B_6$ compounds. The increasing coercivity is our expectation.

Fig. 2(a) and (b) shows the SEM images of random and field-aligned $Pr_{15}Fe_{79}B_6$ flakes prepared by SABM, respectively. It can be seen that the thickness and length of the flakes are mainly in the range of 50 – 200 nm and 0.5–2 μm, respectively. Compared with the random oriented flakes, the field-aligned flakes become well aligned along the direction of the applied magnetic field and form obviously “chains-type” morphology. This result demonstrates that the easy magnetization direction (EMD) of as-milled Pr–Fe–B flakes is parallel to the surface of the flakes.

Fig. 3(a) and (b) shows the XRD patterns of random and field-aligned $Pr_{15}Fe_{79}B_6$ nanoflakes, respectively. It can be seen that the flakes mainly exhibit the tetragonal structure of $Pr_2Fe_{14}B$ (JCPDS PD#40-1156) with minor rare-earth oxides peaks. In addition, the diffraction intensity of (00l) crystalline planes dramatically enhance for the aligned sample whereas the other peaks almost disappear for the random oriented sample, suggesting a (00l) alignment (the EMD along the c-axis). Combining with the result of aligned SEM image (see Fig. 2(b)), we can claim that the c-axis of $Pr_{15}Fe_{79}B_6$ compound is parallel to the surface of the flakes. In order to analyze the texture degree of $Pr_2Fe_{14}B$ nanoflakes, the normalized c-axis alignment degree is calculated for the aligned $Pr_2Fe_{14}B$ nanoflakes/resin composite [7], the value is 98%, and lattice parameters and intensity of diffraction peaks is obtained from Fig. 3, which indicates that the $Pr_2Fe_{14}B$ nanoflakes have a high texture degree.

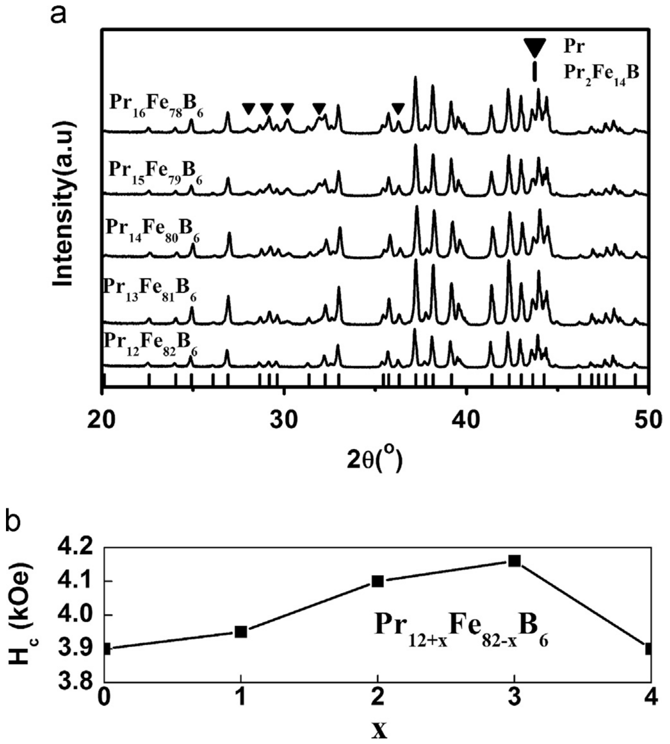

Fig. 1. (a) The measured XRD patterns of starting $Pr_{12+x}Fe_{82-x}B_6$ (x=0, 1, 2, 3, 4) compounds powder and (b) the coercivity of as-milled $Pr_{12+x}Fe_{82-x}B_6$ (x=0, 1, 2, 3, 4) compounds.

Fig. 4(a) shows the angular dependence of half-hysteresis loop for aligned $Pr_{15}Fe_{79}B_6$ nanoflakes/resin composite, where the external field is applied at a certain angle θ with respect to the magnetic aligned axis of the sample. It can be seen that the M_r/M_s reaches 0.9 for the sample with angle $\theta=0°$, which again indicates that the sample have a good alignment degree. The H_c for the aligned sample shows an obviously decrease compared with that of unaligned one (see Fig. 1(b)). It agrees with the theory and experiment result [9,10]. In addition, the H_c firstly increases then decreases with angle θ, and reaches the maximum at 70° (see Fig. 4(b)). These phenomena are also observed for $SmCo_5$ thin films [11], Sm–Co/Fe multilayer films [12] and Sm–Co nanoflakes [13]. The increased H_c agrees with the 1/cosθ law (Kondoraky Law) for an ideal uniaxial system [9] and the later decrease could be due to the magnetization is not saturated. In order to compare the experiment with 1/cosθ law more intuitively, we define the magnetization-related normalized coercovity H_{nc} is as following: $H_{nc}(\theta) = H_c(\theta) \times [M_s/M(2T)]$, where M_s is the magnetization at 2 T with the θ=0°. We can see that H_{nc} has a more similar variation trend compared with 1/cosθ law (see Fig. 4(b)). Generally, the 1/cosθ law is associated with domain wall pinning [9–13]. Therefore, it also indicates that the coercivity of as-milled nanoflakes is mainly dominated by domain wall pinning. However, the difference between the H_{nc} and 1/cosθ can also be observed, especially for the large angle θ, which could be due to the Kondoraky's law does not consider the dipolar interaction. When the magnetostatic energy was calculated in the model, there will be a better agreement between experiment and calculation [9].

In order to further clarify the coercivity mechanism and the possible interaction of $Pr_{15}Fe_{79}B_6$ nanoflakes, the minor hysteresis loops and recoil loops of unaligned $Pr_{15}Fe_{79}B_6$ nanoflakes/resin composite are measured and shown in Fig. 5(a) and (b), respectively. And the inset of Fig. 5(a) shows the normalization of coercivity dependence of the maximum applied field, which is determined from the minor hysteresis loops. It can be seen that the coercivity changes slowly at the low applied fields but increase quickly when the applied field reaches the coercive field (can see more clearly from the first derivative). This generally is a characteristic of the domain wall pinning [12,13]. And it indicates that the coercivity of the as-milled nanoflakes is mainly controlled by domain wall pinning again. It is known that Henkel plots are very important and useful in checking the interaction of particles and the magnetization reversal mechanism, which is defined as: $\delta M = M_d(H) - [1 - 2M_r(H)]$. Here $M_r(H)$ is the isothermal (IRM) remanence (normalized to $M_r(H)/M_r(\infty)$) acquired after the application and subsequent removal of a field H, $M_d(H)$ is dc demagnetizing (DCD) remanence (normalized to $M_d(H)/M_r(\infty)$) acquired after saturation in one direction and then the subsequent application and removal of a direct field H in the reverse direction. The two remanence curves of IRM and DCD are shown in Fig. 6(a), and the data is from Fig. 5(a) and (b), respectively. Many studies have indicated that the IRM and DCD remanence curves can reveal the irreversible energy barrier distribution information, and that

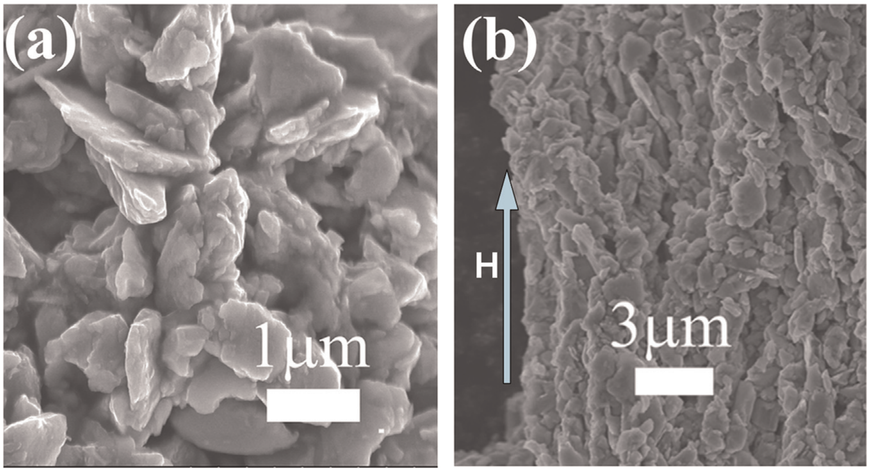

Fig. 2. The SEM images of (a) random and (b) field-aligned $Pr_{15}Fe_{79}B_6$ nanoflakes prepared by SABM.

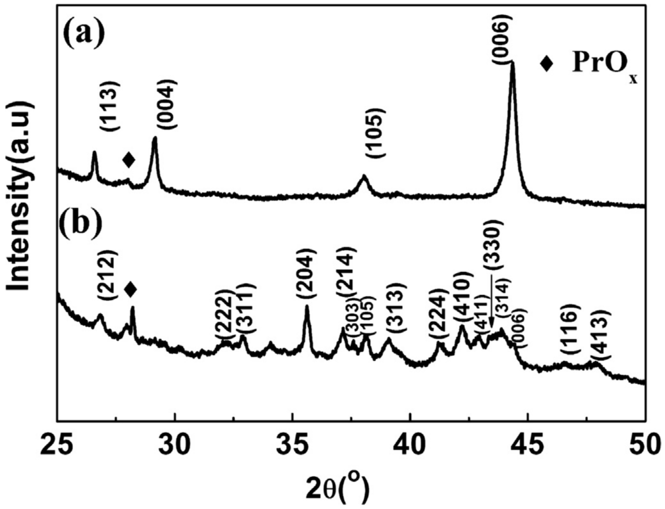

Fig. 3. The XRD patterns of (a) random and (b) field-aligned $Pr_{15}Fe_{79}B_6$ nanoflakes.

the domain wall pinning energy distribution can be determined by the differentiation of the IRM curve, while both the domain wall pinning and nucleation energy distribution can be determined by the differentiation of the DCD curve [14,15]. Fig. 6(b) shows the differentiation curves of the IRM and DCD remanence (normalizing the area of curves to unity). It can be seen that both the energy barrier distributions show a single peak at about 4 kOe and 5 kOe, respectively, and the differential peak of IRM shifts to the right. The results indicate that reversal domain nucleation firstly, and then both nucleation and pinning effect occur, and the coercivity is mainly determined by domain wall pinning. Furthermore, a very large energy barrier distributions overlap can also be observed. This large overlap could be due to the overlap of the nucleation and domain wall pinning energy barrier distribution [14], and it is also mean that nucleation has a very important effect on coercivity, which can be explained by both the close position and similarly intensity of energy barrier distributions [15]. In addition, the broad differential peak can also be observed, which can also further lead to the overlap of energy barrier distribution and is usually caused by demagnetizing effects [14]. According to the Stoner–Wohlfarth model, for a non-interacting single-domain particles, $M_r(H)$ and $M_d(H)$ satisfy the relationship [16–18]: $M_d(H) = 1 - 2M_r(H)$, it is also mean $\delta M = 0$. Therefore, for any $\delta M \neq 0$ in experimental data can be attributed to the effect of interaction. The positive δM imply the interaction attempt to magnetize the materials and usually associated with the exchange couple, while negative δM mean the interaction attempt to demagnetize the materials and usually associated with the dipolar coupling. It can be seen from Fig. 6(c) that the δM shows the negative values under all the fields, indicating the interaction of flakes are mainly dipolar coupling. This can also be demonstrated by the spontaneous formation of “kebab-like” or “chains-type” morphology for as-milled nanoflakes due to the magnetostatic interaction [7,19]. Because of negative value of δM attempt to demagnetize the materials, the strong dipolar coupling could

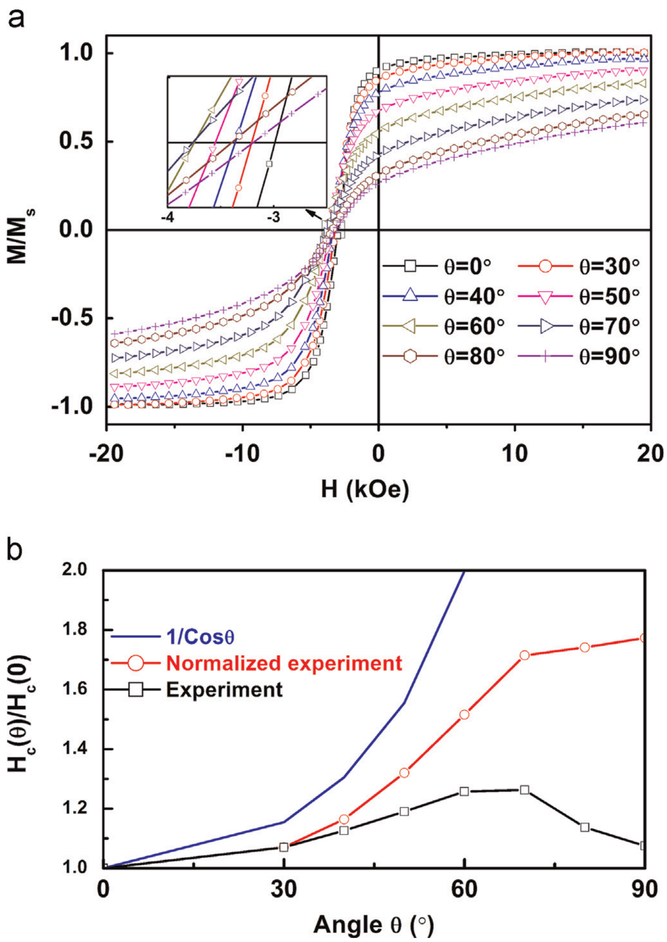

Fig. 4. The angular dependence of (a) half-hysteresis loop and (b) H_c for aligned $Pr_{15}Fe_{79}B_6$ nanoflakes/resin composites.

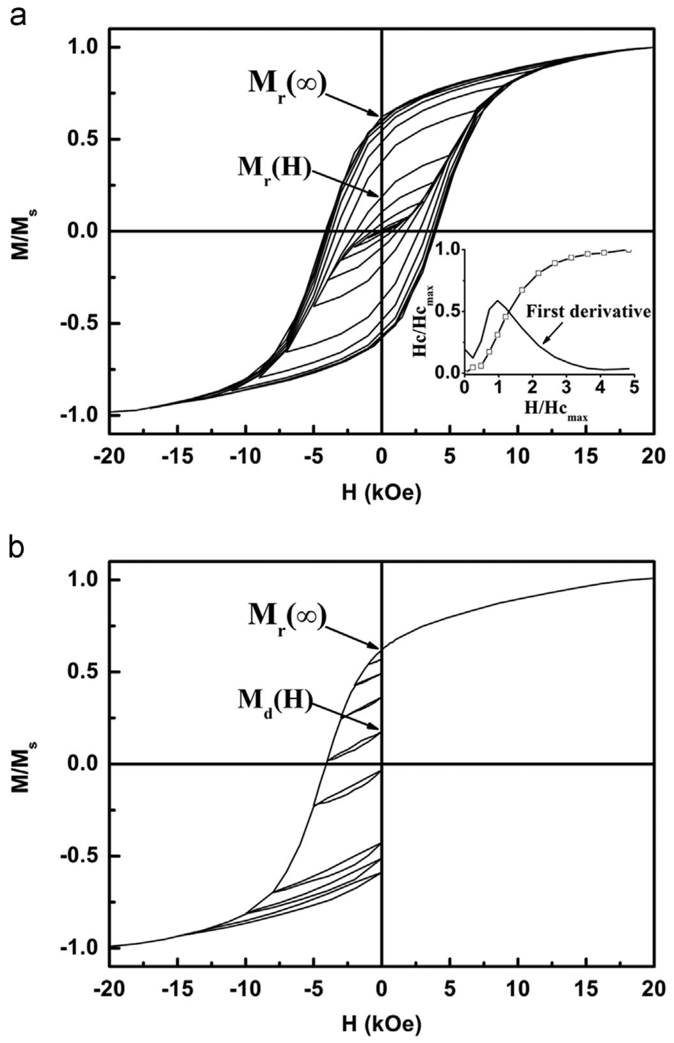

Fig. 5. (a) The minor hysteresis loops and (b) recoil loops of unaligned $Pr_{15}Fe_{79}B_6$ nanoflakes/resin composite, inset of (a) is the normalization of coercivity dependence on the applied field.

decrease the coercivity, which could be one of the causes for the relative low coercivity of as-milled $Pr_{15}Fe_{79}B_6$ nanoflakes. In additions, we found that the δM shows the positive values for the as-milled $PrCo_5$ nanoflakes (it will be shown in another paper), which could explain the relative low coercivity for $R_2Fe_{14}B$ (R=Pr, Nd) nanoflakes while high coercivity for RCo_5 (R=Pr, Sm) nanoflakes. Furthermore, existent strong dipolar coupling also agrees with the experiment result in Fig. 4(b), which is explained in [9]. Therefore, decreasing the negative effect of dipolar coupling could be very useful for obtaining a relative high coercivity.

4. Conclusions

The strong (00*l*) textured $Pr_{12+x}Fe_{82-x}B_6$ (x=0, 1, 2, 3, 4) nanoflakes were prepared by surfactant-assisted ball milling (SABM). A coercivity of 4.16 kOe for $Pr_{15}Fe_{79}B_6$ nanoflakes was obtained, which is the maximum coercivity of $R_2Fe_{14}B$ (R=Pr, Nd) nanoflakes or nanoparticles reported up to now. The angular dependence of coercivity for aligned sample indicates that the coercivity mechanism of the as-milled nanoflakes is mainly dominated by domain wall pinning. Meanwhile, the field dependence of coercivity, IRM remanence and DCD remanence curves indicate that the coercivity is mainly determined by domain wall pinning and

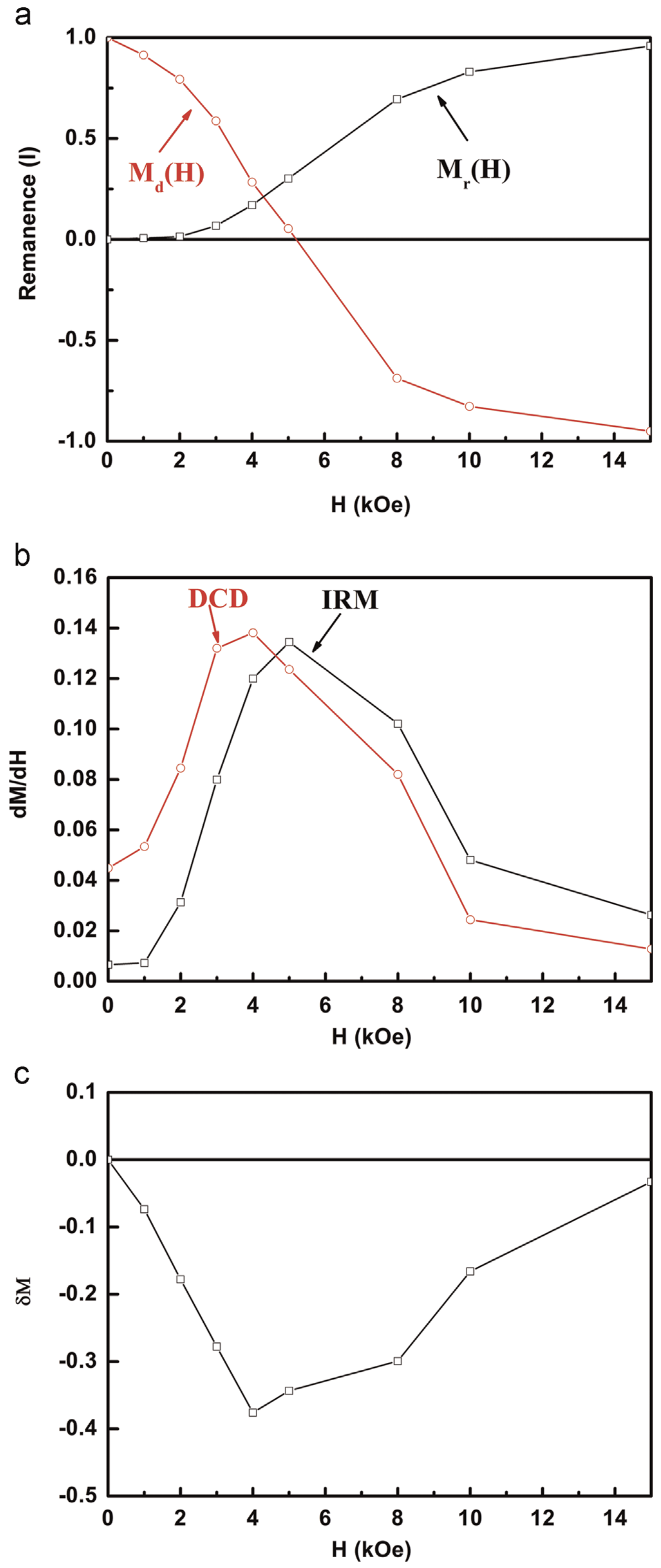

Fig. 6. (a) Field dependence of the IRM and DCD remanence curves, (b) the differentiation curves of the IRM and DCD remanence, and (c) Henkel plots of unaligned $Pr_{15}Fe_{79}B_6$ nanoflakes/resin composite.

nucleation also has a very important effect. In addition, the interaction of flakes is demonstrated mainly to be dipolar coupling, which could be an important cause for the relatively low coercivity of as-milled $Pr_{15}Fe_{79}B_6$ nanoflakes. The research of coercivity mechanism for $Pr_{15}Fe_{79}B_6$ nanoflakes is important for guidance the further increase its value, and is useful for the future development of the high performance nanocomposite magnets and soft/hard exchange spring magnets.

Acknowledgments

This work was supported by the National Basic Research Program of China (Grant no. 2014CB643702). National Natural Science Foundation of China (Grant no. 51401235). Beijing Natural Science Foundation (2152034).

References

[1] S. Sun, C.B. Murray, D. Weller, L. Folks, A. Moser, Science 287 (2000) 1989–1992.
[2] H. Zeng, J. Li, J.P. Liu, Z.L. Wang, S. Sun, Nature 420 (2002) 395–398.
[3] N.G. Akdogan, W. Li, G.C. Hadjipanayis, J. Appl. Phys. 109 (2011) 07A759.
[4] V.M. Chakka, B. Altuncevahir, Z.Q. Jin, Y. Li, J.P. Liu, J. Appl. Phys. 99 (2006) 08E912.
[5] B.Z. Cui, L.Y. Zheng, W.F. Li, J.F. Liu, G.C. Hadjipanayis, Acta Mater. 60 (2012) 1721–1730.
[6] M. Yue, R. Pan, R.M. Liu, W.Q. Liu, D.T. Zhang, J.X. Zhang, X.F. Zhang, Z.H. Guo, W. Li, J. Appl. Phys. 111 (2012) 07A732.
[7] W.L. Zuo, R.M. Liu, X.Q. Zheng, R.R. Wu, F.X. Hu, J.R. Sun, B.G. Shen, J. Appl. Phys. 115 (2014) 17A734.
[8] J. Liu, H. Sepehri-Amin, T. Ohkubo, K. Hioki, A. Hattori, T. Schrefl, K. Hono, Acta Mater. 61 (2013) 5387–5399.
[9] D. Givord, P. Tenaud, T. Viadieu, J. Magn. Magn. Mater. 72 (1988) 247–252.
[10] R.W. Gao, D.H. Zhang, J. Magn. Magn. Mater. 195 (1999) 168–173.
[11] A. Singh, V. Neu, S. Fähler, K. Nenkov, L. Schultz, B. Holzapfel, Phys. Rev. B 77 (2008) 104443.
[12] J. Zhang, Y.X. Li, F. Wang, B.G. Shen, J.R. Sun, J. Appl. Phys. 107 (2010) 043911.
[13] J.W. Nie, X.H. Han, J. Du, W.X. Xia, J. Zhang, Z.H. Guo, A.R. Yan, W. Li, J.P. Liu, J. Magn. Magn. Mater. 347 (2013) 116–123.
[14] T. Thomson, K. O'Grady, J. Phys. D: Appl. Phys. 30 (1997) 1566–1576.
[15] J.B. Wang, Q.F. Liu, D.S. Xue, F.S. Li, Chin. Phys. Lett. 21 (2004) 945–948.
[16] D.E. Speliotis, W. Lynch, J. Appl. Phys. 69 (1991) 4496–4498.
[17] P.D. Mitchler, E.D. Dahlberg, E. Engle, R.M. Roshko, IEEE Trans. Magn. 31 (1995) 2499–2503.
[18] J. Garca-Otero, M. Porto, J. Rivas, J. Appl. Phys. 87 (2000) 7376–7381.
[19] W.L. Zuo, R.M. Liu, X.Q. Zheng, R.R. Wu, F.X. Hu, J.R. Sun, B.G. Shen, J. Appl. Phys. 115 (2014) 17A728.